Multiscale monitoring of interface failure of brittle coating/ductile substrate systems: A non-destructive evaluation method combined digital image correlation with acoustic emission

W. G. Mao, D. J. Wu, W. B. Yao, M. Zhou, and C. Lu

Citation: Journal of Applied Physics **110**, 084903 (2011); doi: 10.1063/1.3651378
View online: https://doi.org/10.1063/1.3651378
View Table of Contents: http://aip.scitation.org/toc/jap/110/8
Published by the American Institute of Physics

Multiscale monitoring of interface failure of brittle coating/ductile substrate systems: A non-destructive evaluation method combined digital image correlation with acoustic emission

W. G. Mao[1,2,3,a)] D. J. Wu[1,3] W. B. Yao,[1,3] M. Zhou,[1,3] and C. Lu[4]
[1]*Key Laboratory of Low Dimensional Materials and Application Technology, Ministry of Education, Xiangtan University, Hunan 411105, China*
[2]*Aeronautical Science and Technology Key Laboratory of Aeronautical Test and Evaluation, Nanchang Hangkong University, Jiangxi 330063, China*
[3]*Faculty of Materials, Optoelectronics and Physics, Xiangtan University, Hunan 411105, China*
[4]*Department of Mechanical Engineering, Curtin University, Western Australia 6845, Australia*

(Received 1 May 2011; accepted 28 August 2011; published online 18 October 2011)

In this paper, we proposed a non-destructive evaluation method combined digital image correlation with acoustic emission techniques. The method was used to *in situ* monitor interface failure and internal damage of brittle coating/ductile substrate systems with different size scales. The results show that there is a good relationship between digital image correlation and acoustic emission signals, which can be applied to judge cracking formation and coating delamination and to determine fracture toughness of a thermal barrier coating system subjected to bending. © *2011 American Institute of Physics*. [doi:10.1063/1.3651378]

I. INTRODUCTION

A system consisting of ductile substrate with functional brittle film/coating layers has been ubiquitous in a variety of applications, such as micro-electronics, ferroelectric actuators, thermal, and abrasion resistance.[1–4] Owing to mismatch of thermo-mechanical properties between film/coating and substrate, however, such a system is always subjected to residual stresses, which would eventually lead to a structural degradation of coating near interfacial regions. Therefore, the way to evaluate the interface adhesion performance of a system and predict its reliability has attracted ever-increasing attention in recent years. To realize optimal design, it is necessary to measure the variation of full/local strain fields, cracking nucleation, propagation, and spallation of a coating/film system during tests. However, it is difficult and inconvenient to accurately obtain information at small size scales with conventional strain gauges, displacement and force sensors, and optical microscopes. Recently, several advanced experimental techniques have been available in the investigations of coating failure and delamination. Atomic force microscopy provides a means of accurate mapping of changes in coating sub-surface that are related to the evolution of debonding.[5] Ultrasonic force microscopy was used to identify the locations of decohesion, which is sensitive to the local variation in mechanical compliance.[6] Scanning electron microscope and thermograph have been utilized to detect the damage evolution.[7,8] Unfortunately, these techniques can only be applied to qualitatively characterize the microstructure variation and cracking morphology of the coating. It is difficult to provide *in situ* quantitative stress/strain information and other detailed damage features to study interfacial properties of a coating/film system. Thus, it is urgent to develop a real-time reliable method to monitor the microscopic failure process of a brittle coating/ductile substrate system and to provide the criteria of coating delamination.

The digital image correlation (DIC) technique, which measures strain fields by tracking random speckle patterns on specimen surface,[9–11] is suitable for continuously detecting micro/nano-scale deformations.[12,13] In addition, accompanied with cracking and coating fracture, the locally stored elastic energy is released in the form of acoustic emission (AE) signals. AE is a passive non-destructive testing technique that relies upon the detection of stress waves propagated through a solid as it undergoes strain. Thus, it is appropriate for monitoring the internal damage evolution of a material.[14,15] In previous works, DIC and AE techniques have been simultaneously applied to study the crack profile, localized plastic strain evolution and full/local strain fields of bulk materials, especially metal alloys with different scales.[16–21] However, precise matches have not been established between AE and DIC techniques to elucidate failure mechanisms of alloys. On the other hand, strain fields and crack profiles of brittle coating/ductile substrate systems are much more complicated than that of bulk materials. To the best of our knowledge, there have been few studies where both DIC and AE techniques are applied to monitor the failure process of multiple coating/film systems.

In this paper, we proposed a combined experimental method of DIC and AE techniques to realize *in situ* tests of the failure process of brittle film/coating systems under bending. The main attention was on how to judge accurately the time and location of cracking formation and coating delamination by synthetically analyzing DIC, AE, and universal testing machine data. A relationship between DIC and AE techniques was established to elucidate interfacial failure mechanisms of brittle coating/ductile substrate systems at small size scales.

[a)]Author to whom correspondence should be addressed. Electronic mail: wgmao@xtu.edu.cn.

II. EXPERIMENTAL

An air plasma sprayed as-received thermal barrier coating (TBC) was selected as a typical brittle coating/ductile substrate system. Well-polished and cleaned SUS304 stainless steel plates of $40 \times 20 \times 2$ mm^3 were used as substrate, on which a Ni–20Cr–10Al–1Y bond coat with thickness of 100 μm and an 8 wt. % Y_2O_3 top coating with thickness of 300 μm were deposited, respectively, by air plasma sprayed technique. The experimental set-up is illustrated in Fig. 1. The total of 10 TBC and 5 uncoated substrate specimens were tested under three-point bending at a speed of 0.1 mm/min using the universal testing machine (REGER 2000), DIC instrument (ARAMIS), and AE equipment (SWAE-5) at room temperature. Prior to DIC testing, stochastic patterns were prepared by spraying a thin layer of black and white paint with airbrush guns. A 1624×1236 pixels charge coupled device camera equipped with a lens of 50 mm focal length was used to *in situ* measure the macroscopic morphology and strain evolution of a region with a sampling rate of 2 images per second. DIC was performed on an image of 4×2 mm^2 to determine local strain fields during loading, as shown with a dashed frame in Fig. 1. The facet size was defined to be 90×90 μm^2 during tests. Post-processing was achieved with the commercially available DIC software (Aramis) to obtain strain data. The measuring error of strain is less than 0.05%.[9,16]

An AE sensor probe with the resonance of 70–400 kHz was located on the side of substrate, which was utilized as a *real-time* continuous monitor to record signal waves released from fracture sources. The AE sampling rate was set to be 1 MHz. The amplitude distribution of AE signals was in the range of 0–100 dB. For TBC tests, we chose 40 dB as the amplitude threshold to avoid the influence of noise and substrate deformation. AE data were analyzed by combining wavelet transform with traditional parameter analysis. The corresponding energy coefficient was calculated by using MATLAB programs with "db8" wavelet.[14] Similarly, the scale was restricted to 5 and all signals were decomposed into 6 levels with the frequency range of D1, D2, D3, D4, D5, and C5.[14] It is found that the peak value of the energy ratio of different frequency bands corresponds to the different failure type, which is similar to the results by Seong *et al.*[22] Therefore, according to the maximum energy ratio among the frequency bands of AE data, the dominant failure or cracking patterns can be determined with the aid of DIC observations. It is worth noting that, however, all experimental apparatus should be *synchronously* performed to validly judge crack nucleation, propagation, and delamination of coating.

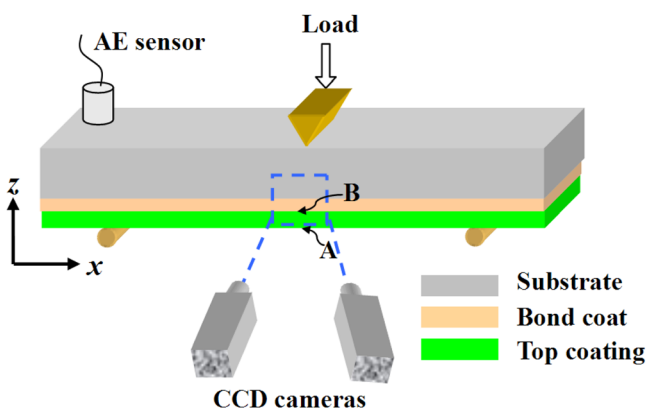

FIG. 1. (Color online) Schematic of three-point bending test with DIC and AE techniques. The rectangle with dashed blue lines was defined as a region for DIC monitoring.

III. RESULTS AND DISCUSSION

A. AE features of uncoated substrate

To consider the influence of uncoated substrate deformation on AE signals of TBCs, the characteristics of AE events and load-deflection-time curve are shown in Fig. 2. It is seen that the amplitude and number of AE signals are weak and small even though substrate experiences elastic and plastic deformation under bending. The wavelet analysis indicates that the dominant frequency band of AE signals is D3 for substrate deformation and its corresponding energy ratio is 0.55.

B. *In situ* monitoring of interface strain

As shown in Fig. 1, the brittle coating was located underneath the substrate, where fracture occurs first due to undertaking the maximum tensile or bending stress. Thus, the subsurface and interface regions were monitored and denoted with A and B, respectively. Based on the analysis of DIC data, three special points L1, L2, and L3 are extracted and marked in the curve of Fig. 3, corresponding to cracking nucleation and coating delamination. For each point, its maps of lateral strain ε_{xx} and longitudinal strain ε_{zz} are displayed and inset in Fig. 3. When the deflection ω is small, strain maps of ε_{xx} and ε_{zz} represent a homogeneous distribution behavior at the early stage (point L1). When ω increases up to 0.38 mm (point L2), the monitor of DIC shows that three apparent strain concentration regions appear close to coating subsurface. With the increase of ω, micro-cracks rapidly propagated toward the coating/substrate interface and other strain concentration regions continued to initiate

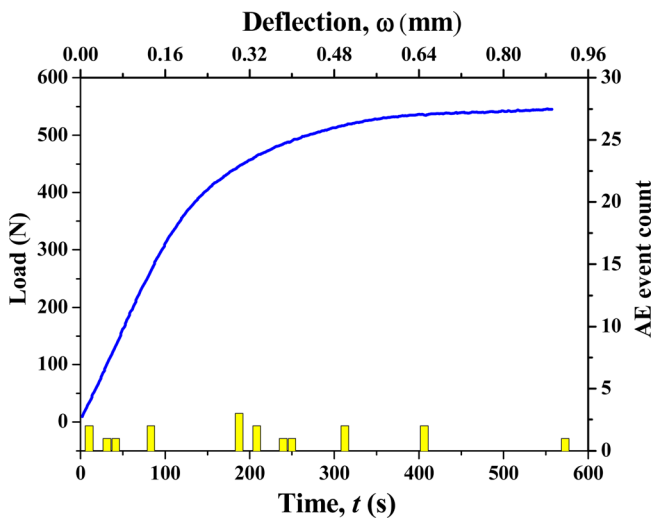

FIG. 2. (Color online) The distribution of AE events of uncoated substrate vs test time and the corresponding loading-deflection curve during bending.

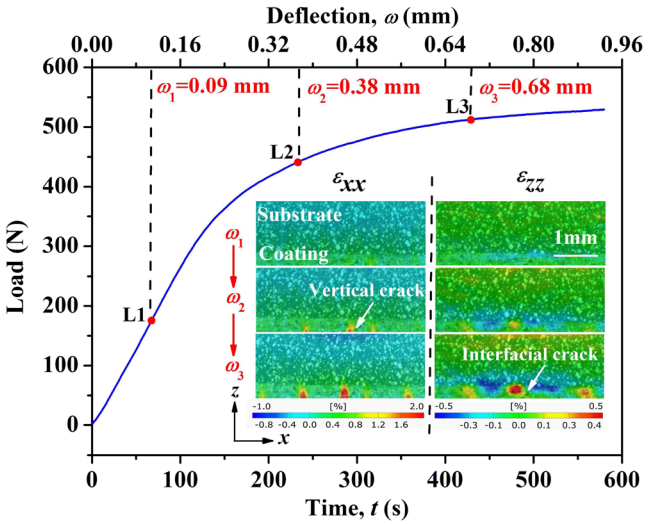

FIG. 3. (Color online) A typical loading-deflection-time curve of TBCs under bending. A series of strain map insets show the evolution of lateral and longitudinal strains in the monitored area with the increase of ω, as shown in Fig. 1. Here, ω at three points L1, L2, and L3 are equal to, respectively, 0.09, 0.38, and 0.68 mm.

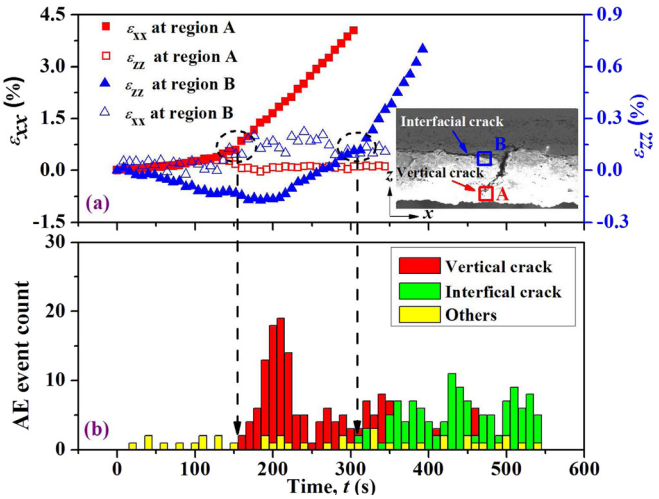

FIG. 4. (Color online) The evolution of local strain and AE signals as a function of loading time during bending tests. (a) The variations of ε_{xx} and ε_{zz} with test time provided by DIC, and (b) the distributions of three different kinds of AE signals with test time corresponding to different failure types.

near the coating subsurface region, as indicated in inset of strain maps at $\omega_3 = 0.68$ mm (point L3). The DIC micro-observations clearly reveal that vertical cracks firstly form near the coating subsurface and then propagate to the coating/substrate interface as bending load increases. Once arriving at the interface, they gradually deflect into interface cracks and start to propagate within coating along the interface direction. Eventually, the number of surface vertical cracking stops increasing and goes into a saturation state. Partial interface cracks result in coating delamination and subsequent spallation. Thus, there are two main types of cracking patterns: surface vertical cracks and interface cracks (see inset in Fig. 3).

C. Failure modes and AE measurements

The local stored elastic energy in coating would release due to cracking formation and coating fracture. The evolution of local strain and AE data of two regions A and B were extracted and re-plotted in Figs. 4(a) and 4(b), respectively. For region A, the magnitude of ε_{xx} gradually increases with the increase of ω. The result of a randomly selected AE signal before coating cracking shows that the dominant frequency band of AE signals is D3 and the corresponding energy ratio is 0.55, as presented in Figs. 5(a) and 5(b), respectively, which means that AE signals are mainly ascribed to substrate deformation before cracking nucleation. It is interesting to observe an abrupt transition at $\varepsilon_{xx} = 0.75\%$ when the loading time $t = 152$ s, which implies a surface vertical crack formation in region A. The wavelet analysis of recorded AE data indicates that AE signals change from a single type into two completely different modes (see Fig. 4(b)). The related dominant frequency band of AE signals changes from D3 into D1 and its energy ratio is 0.62, as shown in Figs. 5(c) and 5(d). It clarifies that before $t = 152$ s, AE signals are substrate deformation, as marked with yellow in Fig. 4(b). But after $t = 152$ s, two AE signals are composed by surface vertical cracks and substrate deformation. The new AE events are labeled by red in Fig. 4(b). It is obvious that the amplitude and energy of cracking AE signals are much more than that of substrate deformation. When ω increases, similar surface vertical cracks occur close to coating subsurface and then propagate toward the coating/substrate interface. It is observed from DIC data that the evolution of ε_{zz} in region B displays an apparent excursion and changes from compressive to tensile states at $t = 312$ s. The reason may be that, after the first vertical crack in region A reaches at the coating/substrate interface (region B), it transformed into a new interface crack. Simultaneously, the analysis of AE signals indicates that there appears another new kind of AE event marked with green in Fig. 4(b). In this phase, the dominant frequency band of AE signals turns from D1 into D2 and the corresponding energy ratio is 0.75, as shown in Figs. 5(e) and 5(f), respectively. Finally, as ω increases, brittle coating may break into a few small segmented coatings when different interface cracks link with each other. Based on the wavelet transform with traditional parameters and DIC micro-observations, the major features of AE signals of TBCs can be divided into three different phases, including no cracking, surface vertical cracks, and interface cracks. Therefore, the related border lines can be determined by these special test time points, as shown in Fig. 4(b). The correlation between DIC and AE data as a function of test time can be established, which is utilized to accurately judge cracking formation and coating delamination of coating/film systems. More importantly, such a method can be used to obtain critical experimental data near transition points, which are crucial to deduce mechanical properties of coating/film systems, such as interface adhesion strength, fracture toughness, and energy release rate.

D. Evaluation of interface fracture toughness

Using the critical experimental data obtained above, a shear-lag model was introduced to estimate the fracture

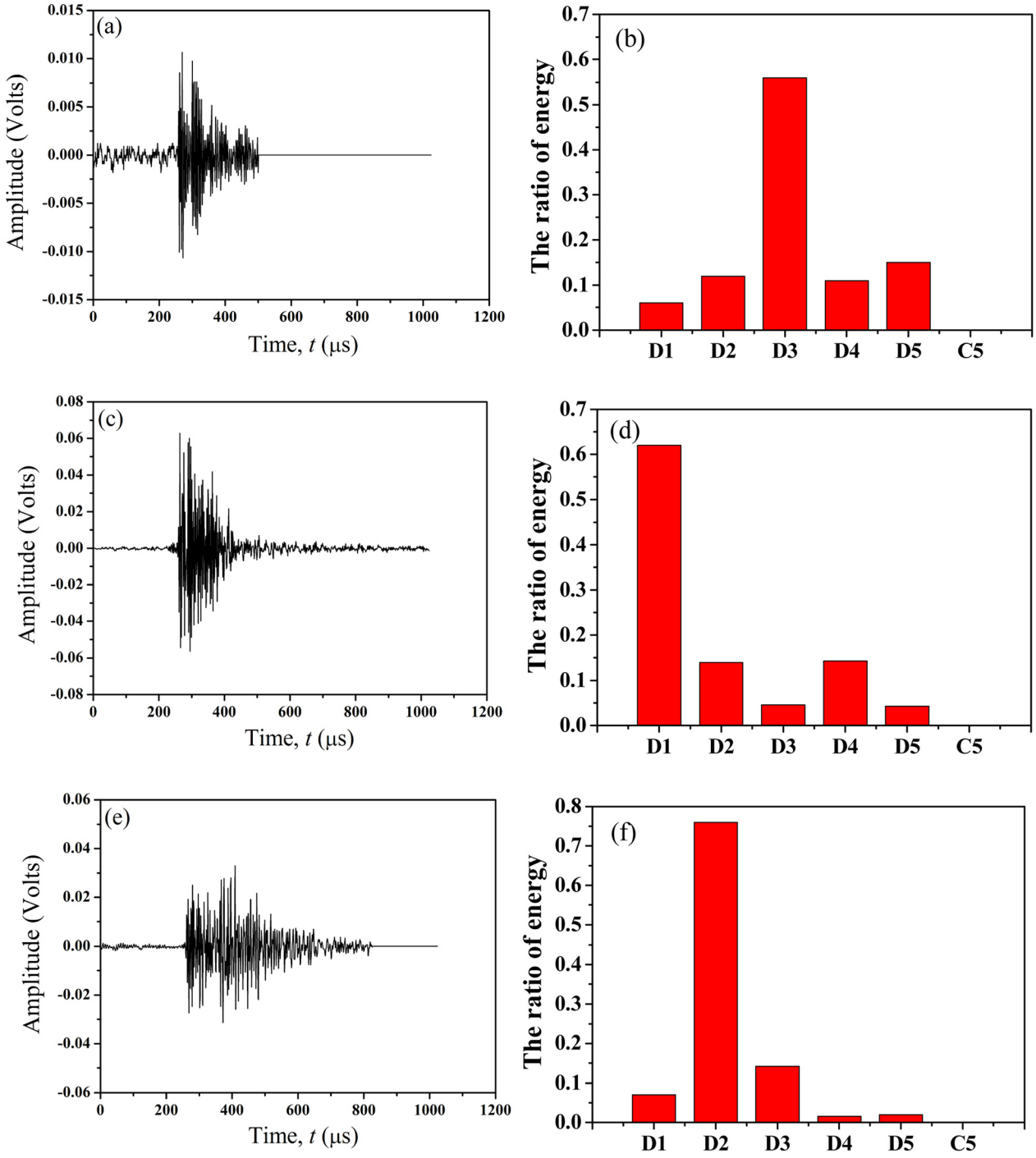

FIG. 5. (Color online) Three typical AE waveforms extracted from different test time points in Fig. 4(b), i.e. (a) primary phase, (c) $t = 152$ s, and (e) $t = 312$ s, respectively. Figures (b), (d), and (f) are their energy coefficient ratios after wavelet analysis.

toughness of TBCs.[23,24] In our tests, deflection is currently restricted within a very small range. Assumed that the segmented coating mainly undertakes tensile stress,[25] as illustrated in Fig. 6, the stress distribution in a coating segment can be written as[26]

$$\sigma_c(x) = E_c \varepsilon_s \left[1 - \frac{\cosh(x/\xi)}{\cosh(\lambda/2\xi)}\right], \tag{1}$$

where λ and $\sigma_c(x)$ are length and tensile stress of the segmented coating, respectively, ε_s is average tensile strain in the substrate, and ξ is defined as $\xi = \sqrt{E_c d_1 d_2 / G_i}$. Here, E_c is Young's modulus of coating and G_i is the shear modulus of the interlayer, and d_1 and d_2 are the thicknesses of the coating and interlayer, respectively. The strain energy accumulated in the coating segment per unit length under tensile stress can be approximated by

$$U = \int_{-\frac{\lambda}{2}}^{\frac{\lambda}{2}} \frac{\sigma_c^2(x) d_1}{2E_c} 2dx. \tag{2}$$

Inserting Eq. (1) into Eq. (2), the strain energy is

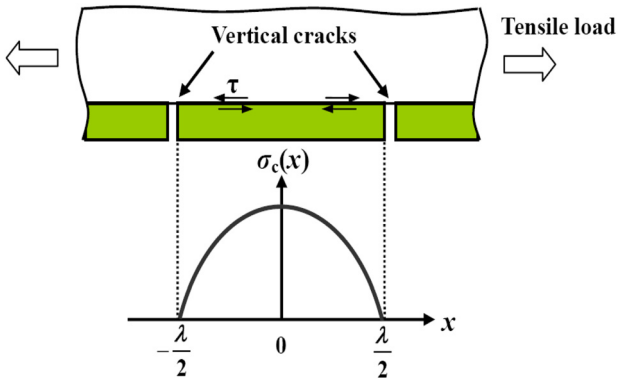

FIG. 6. (Color online) Schematic of the shear lag model for a segmented coating.

$$U = \frac{E_c \varepsilon_s^2 d_1}{2}\left[\lambda + \frac{\lambda}{1+\cosh(\lambda/\xi)} - 3\tanh(\lambda/2\xi)\right]. \quad (3)$$

As the length a of the interface delamination grows, the length of the bonded part is reduced as $\lambda = \lambda_o - 2a$, where λ and λ_o denote the current and initial lengths of the bonded coating. For simplicity, it is assumed that only the strain energy in coating drives delamination.[27] Then, the energy release rate G associated with interface delamination can be written as

$$G = -\frac{\partial U}{\partial a} = \frac{E_c \varepsilon_s^2 d_1}{2}\left\{2 + \frac{2}{1+\cosh[(\lambda_o - 2a)/\xi]} - 3\sec h^2\left(\frac{\lambda_o - 2a}{2\xi}\right) + \frac{2(\lambda_o - 2a)\sinh[(\lambda_o - 2a)/\xi]}{\xi[1+\cosh[(\lambda_o - 2a)/\xi]]^2}\right\}. \quad (4)$$

Thus, the interface fracture toughness G_c can be deduced based on the delamination onset strain ε_{crit} at $a = 0$. For an as-received TBC system, $E_c = 10\,\text{GPa}$,[28] $G_i = 4.5\,\text{GPa}$, $d_1 = 300\,\mu\text{m}$, $d_2 = 100\,\mu\text{m}$, λ_o =0.83-1.16 mm, and $\varepsilon_{crit} = 0.64$–$0.72\%$ by DIC measurements. The interface fracture toughness of TBCs was estimated to be 103–129 J/m^2 by Eq. (4), which are in agreement with the available results.[29,30]

IV. CONCLUSIONS

The interface failure characteristics of TBCs were studied by bending tests with the aid of DIC and AE techniques. An important correlation between DIC and AE was established as a function of test time, which can be used to judge cracking nucleation and coating delamination of TBCs. Compared with traditional strain measurements and crack observation methods, this non-destructive measurement method has an advantage in dynamically monitoring the coating/film failure and assessing their reliabilities at different size scales. Using crucial experimental data, the fracture toughness of top coating/bond coat interface was estimated to be 103-129 J/m^2 by a shear-lag model. Such a method can be also applied in non-destructive *real-time* evaluation of mechanical characteristics of bulk and coating/film materials at high temperatures.

ACKNOWLEDGMENTS

We are grateful to Dr. L. Yang for helpful discussion on acoustic emission detection and data analysis. This work has been supported by the Open Fund of Aeronautical Science and Technology Key Laboratory of Aeronautical Test and Evaluation of Nanchang Hangkong University (No. HK2009005), the Young Teacher Fund of Ministry of Education (No. 200805301023), the foundation of teaching and research equipment transformation development project (SG2009001), and the National Natural Science Foundations of China (No. 11102177 and 10828205).

[1] S. Gupta, Q. Zhang, T. Emrick, A. C. Balazs, and T. P. Russell, Nature Mater. **5**, 229 (2006).
[2] N. Holten-Andersen, G. E. Fantner, S. Hohlbauch, J. H. Waite, and F. W. Zok, Nature Mater. **6**, 669 (2007).
[3] N. P. Padture, M. Gell, and E. H. Jordan, Science **296**, 280 (2002).
[4] X. L. Zhong, J. B. Wang, L. Z. Sun, C. B. Tan, X. J. Zheng, and Y. C. Zhou, Appl. Phys. Lett. **90**, 012906 (2007).
[5] M. George, C. Coupeau, J. Colin, and J. Grilhé, Thin Solid Films **429**, 267 (2003).
[6] A. P. McGuigan, B. D. Huey, G. A. D. Briggs, O. V. Kolosov, Y. Tsukahara, and M. Yanaka, Appl. Phys. Lett. **80**, 1180 (2002).
[7] L. Qian, S. Zhu, Y. Kagawa, and T. Kubo, Surf. Coat. Technol. **173**, 178 (2003).
[8] E. P. Busso, L. Wright, H. E. Evans, L. N. McCartney, S. R. J. Saunders, S. Osgerby, and J. Nunn, Acta Mater. **55**, 1491 (2007).
[9] D. J. Wu, W. G. Mao, Y. C. Zhou, and C. Lu, Appl. Surf. Sci. **257**, 6040 (2011).
[10] T. Chu, W. Ranson, and M. Sutton, Exp. Mech. **25**, 232 (1985).
[11] P. Luo, Y. Chao, M. Sutton, and W. Peters, Exp. Mech. **33**, 123 (1993).
[12] C. C. Aydiner, D. W. Brown, N. A. Mara, J. Almer, and A. Misra, Appl. Phys. Lett. **94**, 031906 (2009).
[13] A. Fedorov, W. P. Vellinga, and J. T. M. D. Hosson, J. Appl. Phys. **103**, 103523 (2008).
[14] L. Yang, Y. C. Zhou, W. G. Mao, and C. Lu, Appl. Phys. Lett. **93**, 231906 (2008).
[15] S. A. Catledge, Y. K. Vohra, S. Woodard, and R. Venugopalan, Appl. Phys. Lett. **82**, 1625 (2003).
[16] H. Louche, K. Bouabdallah, P. Vacher, T. Coudert, and P. Balland, Exp. Mech. **48**, 741 (2008).
[17] H. Jiang, F. A. Garcia-Pastor, D. Hu, X. Wu, M. H. Loretto, M. Preuss, and P. J. Withers, Acta Mater. **57**, 1357 (2009).
[18] J. Kovac, C. Alaux, T. J. Marrow, E. Govekar, and A. Legat, Corros. Sci. **52**, 2015 (2010).
[19] R. Pullin, M. J. Eaton, J. J. Hensman, and K. M. Holford, Appl. Mech. and Mater. **24–25**, 221 (2010).
[20] S. V. Panin, A. V. Byakov, V. V. Grenke, I. V. Shakirov, and S. A. K. Yussif, Phys. Mesomech. **13**, 203 (2010).
[21] X. Sun, K. S. Choi, W. N. Liu, and M. A. Khaleel, Int. J. Plast. **25**, 1888 (2009).
[22] S.-H. Seong, S. Hur, J.-S. Kim, J.-T. Kim, W.-M. Park, U.-C. Lee, and S.-K. Lee, Ann. Nucl. Energy **32**, 479 (2005).
[23] S. Frank, U. A. Handge, S. Olliges, and R. Spolenak, Acta Mater. **57**, 1442 (2009).
[24] X. C. Zhang, B. S. Xu, H. D. Wang, and Y. X. Wu, J. Appl. Phys. **100**, 113525 (2006).
[25] X. F. Zhu, B. Zhang, J. Gao, and G. P. Zhang, Scr. Mater. **60**, 178 (2009).
[26] A. P. McGuigan, G. A. D. Briggs, V. M. Burlakov, M. Yanaka, and Y. Tsukahara, Thin Solid Films **424**, 219 (2003).
[27] S. Tarasovs, J. Andersons, and Y. Leterrier, Acta Mater. **58**, 2948 (2010).
[28] W. G. Mao, Q. Chen, C. Y. Dai, L. Yang, Y. C. Zhou, and C. Lu, Surf. Coat. Technol. **204**, 3573 (2010).
[29] Y. Yamazaki, A. Schmidt, and A. Scholz, Surf. Coat. Technol. **201**, 744 (2006).
[30] S. S. Kim, Y. F. Liu, and Y. Kagawa, Acta Mater. **55**, 3771 (2007).